

# In vitro cytotoxicity screening of water-dispersible metal oxide nanoparticles in human cell lines

Jong Young Choi · Su Hee Lee · Hyon Bin Na · Kwangjin An · Taeghwan Hyeon · Tae Seok Seo

Received: 31 May 2009 / Accepted: 13 July 2009 / Published online: 28 July 2009  
© Springer-Verlag 2009

**Abstract** In this study, we present in vitro cytotoxicity of iron oxide ( $\text{Fe}_3\text{O}_4$ ) and manganese oxide (MnO) using live/dead cell assay, lactate dehydrogenase assay, and reactive oxygen species detection with variation of the concentration of nanoparticles (5–500  $\mu\text{g}/\text{ml}$ ), incubation time (18–96 h), and different human cell lines (lung adenocarcinoma, breast cancer cells, and glioblastoma cells). The surface of nanoparticles is modified with polyethyleneglycol-derivatized phospholipid to enhance the biocompatibility, water-solubility, and stability under an aqueous media. While the cytotoxic effect was negligible for 18 h incubation even at highest concentration of 500  $\mu\text{g}/\text{ml}$ , MnO nanoparticle represented higher level of toxicity than those of  $\text{Fe}_3\text{O}_4$  and the commercial medical contrast reagent, Feridex after 2 and 4 day incubation time. However, the cytotoxicity of  $\text{Fe}_3\text{O}_4$  is equivalent or better than Feridex based on the live/dead cell viability assay. The engineered MnO and  $\text{Fe}_3\text{O}_4$  exhibited excellent stability compared with Feridex for a prolonged incubation time.

**Keywords** Water-dispersible  $\text{Fe}_3\text{O}_4$  and MnO nanoparticle · Magnetic resonance imaging contrast agents · Cytotoxicity · Nanotoxicology

## Introduction

Nanoscale structures and materials have been explored in many biological applications because of their novel optical and electronic properties that differ from their bulk counterparts. Besides, high volume/surface ratio, surface tailor-ability, and multifunctionality allow nanoparticles as an ideal probe for molecular and cellular imaging. As the nanotechnology has expanded its application to biomedicine and biomedical areas, nanotoxicology is emerged to elucidate the relationship of the physical and chemical properties (size, shape, surface chemistry, composition, and aggregation) of nanostructures with induction of toxic biological responses [1]. In the field of biomedicine, nanoparticles are used as efficient diagnostic and therapeutic tools to detect and treat human diseases, but the small size of the nanoparticles typically less than 100 nm has generated greater concerns in terms of risks to human health and the environments [2–4]. For clinic adaptation and commercialization of such nanoparticles, screening of cytotoxicity effect should be performed, since toxicity is a critical factor to consider when evaluating their potential. Although the in vivo use of nanoparticles requires thorough understanding of the kinetics and toxicology of the particles and in vitro experiments must have in vivo validation in order to be useful, the in vitro cytotoxicity studies are being increasingly performed since they are simpler, faster, and less expensive than their in vivo counterparts [5–8]. For nanoparticles to move into the clinical arena, it is important that nanotoxicology research understands how the multiple factors such as nanoparticle size and composition, surface coating, different cell lines, incubation time, and colorimetric assays influence the toxicity of nanoparticles so that their undesirable properties can be avoided.

J. Y. Choi · S. H. Lee · T. S. Seo (✉)  
Department of Chemical and Biomolecular Engineering  
(BK21 Program) and Institute for the BioCentury, KAIST,  
Daejeon 305-701, Korea  
e-mail: seots@kaist.ac.kr

H. B. Na · K. An · T. Hyeon  
National Creative Research Initiative Center for Oxide  
Nanocrystalline Materials, School of Chemical and  
Biological Engineering, Seoul National University,  
Seoul 151-744, Korea

A representative example of nanoparticle application for biomedicine is magnetic nanoparticles for contrast-enhancement agents for MRI to provide excellent anatomical images. In our previous study, novel metal oxide nanoparticles such as iron oxide ( $\text{Fe}_3\text{O}_4$ ) and manganese oxide ( $\text{MnO}$ ) were shown to overcome the drawbacks of currently used MRI contrast agents and specifically target and image breast cancer cells in a mouse brain [9]. A key requirement for the successful use of these nanoparticles in biomedical applications is their good dispersity, colloidal stability in biological media, internalization efficiency, and low toxicity. Recently, various methods for synthesizing high-quality metal oxide nanoparticles with improved monodispersity and crystallinity have been reported [10–12]. However, such nanoparticles are water-immiscible and not sufficiently stable for biomedical applications. Therefore, the development of a method for modifying the surface of these nanoparticles in order to endow them with better water-dispersibility, stability, and biocompatibility is essential for extensive biomedical use [13–15]. Quite recently, several surface modification methods of rendering magnetic ferrite nanoparticles water-dispersible have been reported. Most of these studies focused on passivating the nanoparticles with silica or polymer shells [16–18]. As the metal oxide surface is so stable and unreactive that limited strategies to make nanoparticles water-soluble are possible. In this study, we used the polyethyleneglycol (PEG)-derivatized phospholipid ligands with biocompatible PEGs as tail groups and surface coordinating phospholipids as head groups for the purpose of displacing the hydrophobic ligands on the surface of the metal oxide nanoparticles, thereby stabilizing them in an aqueous media [9, 19]. Another advantage of this sophisticated approach is not dependent on the core materials of nanoparticles, enabling any type of inorganic nanoparticles to be modified by PEG-phospholipid. With these PEG-phospholipid encapsulated  $\text{Fe}_3\text{O}_4$  (12 nm diameter) and  $\text{MnO}$  (14 nm diameter) nanoparticles, we performed the *in vitro* cytotoxicity screening using live/dead cell assay, lactate dehydrogenase (LDH) assay, and reactive oxygen species (ROS) detection kit to infer the cytotoxic mechanism for cell damage that nanoparticles caused. Epithelial cells of lung adenocarcinoma (A549), breast cancer cells (MCF7), and glioblastoma cells (T98G) were selected as *in vitro* models to assess nanocellular toxicity, as MRI contrast agents have potential impact on those cell lines *in vivo*. The effect of concentration of nanoparticles and incubation time on the cytotoxicity was evaluated compared with that of a commercial medical contrast reagent, Feridex. Even though *in vitro* experiments must have *in vivo* validation in order to be meaningful, simple *in vitro* toxicity models and assays may provide the general sense of toxicity in a relatively

short time and assist subsequent toxicity risk assessment of nanoparticles.

## Materials and methods

### Synthesis of water-dispersed $\text{Fe}_3\text{O}_4$ and $\text{MnO}$ nanoparticles

Water-dispersible and biocompatible  $\text{Fe}_3\text{O}_4$  and  $\text{MnO}$  nanoparticles were prepared by the method described previously with some modifications [9, 12, 19]. Uniform-sized  $\text{Fe}_3\text{O}_4$  and  $\text{MnO}$  nanoparticles dispersed in nonpolar organic solvent were synthesized by the thermal decomposition of Fe-oleate and Mn-oleate complexes, respectively [12].

The resulting  $\text{Fe}_3\text{O}_4$  and  $\text{MnO}$  nanoparticles dispersed in chloroform were then encapsulated by PEG-phospholipids shell to endow them with biocompatibility. Typically, 2 ml of the organic dispersible oxide nanoparticles in  $\text{CHCl}_3$  (5 mg/ml) was mixed with 1 ml of  $\text{CHCl}_3$  containing 10 mg of 1, 2-distearoyl-*sn*-glycero-3-phosphoethanolamine-*N*-[methoxy(polyethylene glycol)-2000] (mPEG-2000 PE, Avanti Polar Lipids, Inc.). After evaporating solvent, it was incubated at 70°C in vacuum for 1 h. The addition of 5 ml water resulted in a clear and dark-brown suspension. After filtration, excess mPEG-2000 PE was removed by ultracentrifugation. Resulting nanoparticles were well dispersed in phosphate buffered saline (PBS, pH 7.2).

### Cell culture and treatment with nanoparticles

The human cancer cell lines were derived from the epithelial cells of lung adenocarcinoma (A549, ATCC CCL-185), breast cancer cells (MCF7, ATCC HTB-22), and glioblastoma cells (T98G, ATCC CRL-1690). Growth properties of all cell lines used in this study are as adherent cells and used between subculture passages 5 and 15. The cell lines were maintained in Dulbecco's-Modified Eagle's Medium (DMEM, Invitrogen, Eugene, OR, USA) containing 10% fetal bovine serum (FBS, Invitrogen, Eugene, OR, USA) and 1% mixture of  $10^4$  units/ml penicillin and 10 mg/ml streptomycin (Invitrogen, Eugene, OR, USA). Subsequently, cells were grown and maintained in T-75 cell culture flask at 37°C in a 5%  $\text{CO}_2$  humidified incubator (HERAcell<sup>®</sup> 150, Thermo electron corporation, Asheville, USA) with 80–90% confluence before cell detaching and subculture. After the process of washing with phosphate buffered saline (PBS, Invitrogen, Eugene, OR, USA), cells were incubated in 3 ml of 0.2% trypsin-ethylenediaminetetraacetic acid (trypsin-EDTA, Invitrogen, Eugene, OR, USA) for 3–5 min at 37°C in  $\text{CO}_2$

incubator. Cell suspensions were centrifuged for 3 min at 1,300 rpm. The pellet was re-suspended with fresh DMEM and the seed density was adjusted using a disposable hemocytometer (SKC Co. Ltd., Seoul, Korea) based cell counting with the aid of an inverted microscope (Nikon SMZ 1500 microscope, Tokyo, Japan). Cells were cultured in 8- or 96-well plates for confluent exposures with Fe<sub>3</sub>O<sub>4</sub> and MnO nanoparticles. The cells were treated with various concentrations of nanoparticles according to the time schedule, which are designated in the following sections of each cytotoxicological study.

#### Cell viability tests using a laser scanning confocal microscope

Cell viability was measured by live/dead cell assay (Live/Dead<sup>®</sup> Viability/Cytotoxicity Kit, Invitrogen, Eugene, OR, USA). Cells (A549 and MCF7) were seeded on 96-well tissue culture plates with  $1 \times 10^4$  cells in 100  $\mu$ l media per well. After 24 h stabilization of the cells, they were treated with 5, 50, and 500  $\mu$ g/ml concentrations of nanoparticles (Fe<sub>3</sub>O<sub>4</sub>, MnO, and Feridex) for 18 h. At the end of the exposure, the cells were washed with PBS followed by the addition of 2  $\mu$ M calcein acetoxymethyl (Calcein AM) and 4  $\mu$ M ethidium homodimer-1 (EthD-1). After a brief incubation of 30 min at 37°C, the cells were visualized using a laser scanning confocal microscope (LSM 510—Mets NLU, Carl Zeiss, Oberkochen, Germany) with excitation and emission of green (ex/em 494/530 nm for Calcein AM) and red (ex/em 528/645 nm for EthD-1) fluorescence.

#### Cell viability tests using a microplate spectrofluorometer

Cytotoxicity of the cells (A549, MCF7, and T98G) was measured by live/dead cell assay. Cell lines were seeded on 96-well tissue culture plates with  $1 \times 10^3$ – $5 \times 10^3$  cells in 100  $\mu$ l media per well. Cells incubated for 24 h after seeding were pretreated initially with 500  $\mu$ g/ml of nanoparticles such as Fe<sub>3</sub>O<sub>4</sub>, MnO, and commercial contrast reagent Feridex (Feridex I.V.<sup>®</sup>, TAEJOON pharmaceutical Co. Ltd., Seoul, Korea) for 2 and 4 days. Treated cell samples were washed with PBS and then incubated with 2  $\mu$ M calcein AM and 4  $\mu$ M EthD-1 for 30 min. At the end of the incubation, culture plates were read under a microplate spectrofluorometer (Spectra Max M2, Molecular Devices, CA, USA) with excitation and emission of green (ex/em 494/530 nm for Calcein AM) and red (ex/em 528/645 nm for EthD-1) fluorescence. Each experiment was repeated in quadruplicate, and mean and standard deviation were calculated.

#### Lactate dehydrogenase (LDH) leakage assay

The leakage of lactate dehydrogenase (LDH) in A549, MCF7, and T98G cells were determined using a LDH assay (DHL<sup>™</sup> Cell Cytotoxicity Assay Kit, Anaspec, San Jose, CA, USA). Initially, cells were seeded on 96-well tissue culture plates with  $1 \times 10^3$ – $5 \times 10^3$  cells in 100  $\mu$ l media per well. After 24 h stabilization of the cells, they were treated with 500  $\mu$ g/ml concentrations of nanoparticles (Fe<sub>3</sub>O<sub>4</sub>, MnO, and Feridex) for 2 and 4 days. At the end of exposure, cells were washed with PBS and incubated with 15  $\mu$ l/well of lysis solution for 2 min. Subsequently, it was followed by the addition of 30  $\mu$ l LDH assay solution supported by the assay kit and incubated for 10 min at 25°C. At the end of the incubation, cells were read under a microplate spectrofluorometer with an excitation 545 nm and an emission of 590 nm.

#### Reactive oxygen species (ROS) detection

The generation of reactive oxygen species (ROS) was recorded in A549 cells treated with MnO nanoparticles using ROS kit (Image iT<sup>™</sup> LIVE Green Reactive Oxygen Species Detection Kit, Invitrogen, Eugene, OR, USA). Cell lines incubated for 24 h after seeding were pretreated with 5, 50, and 500  $\mu$ g/ml concentrations of MnO nanoparticles for 1, 2, and 4 days. Later, cells were washed with PBS and then incubated with 20  $\mu$ M 5-(and-6)-carboxy-2',7'-dichlorodihydrofluorescein diacetate (carboxy-H<sub>2</sub>DCFDA) for 30 min at 37°C. At the end of the incubation, cells were washed again with PBS and visualized using a laser scanning confocal microscope with an excitation 495 nm and an emission of 529 nm.

## Results and discussion

### Characterization of synthesized nanoparticles

Water-dispersible iron oxide (Fe<sub>3</sub>O<sub>4</sub>) and manganese oxide (MnO) nanoparticles were prepared by the reported method with some modifications (Fig. 1) [9, 12, 19]. This method is using the hydrophobic interaction between the surfactants stabilizing nanoparticles and phospholipids like liposome preparation. At first, uniform-sized oxide nanoparticles were synthesized by the thermal decomposition of metal–oleate complex [12]. As resulting nanoparticles were stabilized by hydrophobic tails of surfactants (oleic acid and oleylamine), they were dispersed in nonpolar organic solvent such as chloroform. They were then encapsulated by PEG–phospholipids shell to endow them with biocompatibility [19]. Figure 2 shows the transmission electron

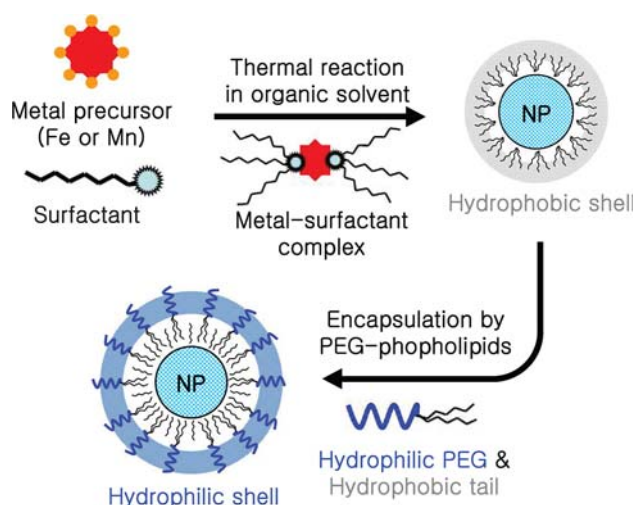


**Fig. 1** Schematic illustration for water-dispersible oxide nanoparticle synthesis. Monodisperse nanoparticles coated by hydrophobic tails of surfactants are produced in thermal decomposition process and then encapsulated by PEG–phospholipids shell

microscopic (TEM) images of monodisperse  $\text{Fe}_3\text{O}_4$  (12 nm dia.) and  $\text{MnO}$  (14 nm dia.) nanoparticles in inorganic core size without organic surfactants or PEGs. After modification with lipid–PEGs, hydrodynamic diameters of coated nanoparticles were measured, which are larger than the sizes in TEM image due to swelling of PEG–shell in water. This result demonstrates realistic size of encapsulated nanoparticles, and well dispersity without any aggregation in an aqueous solution that are indispensable requirements for cytotoxicity evaluation to obtain consistent and reproducible data.

#### Viability survey using live/dead cell assay

Live/dead cell assay kit provides a two-color fluorescence in cell viability test that is based on the simultaneous determination of live and dead cells with two probes that measure recognized parameters of cell viability; intracellular esterase activity, and plasma membrane integrity. Live cells are distinguished by presence of ubiquitous intracellular esterase activity, determined by the enzymatic conversion of the virtually nonfluorescent cell-permeant calcein AM to the intensely green fluorescent calcein [20–22]. On the other hand, EthD-1 enters cells through damaged membranes and undergoes a 40-fold enhancement of fluorescence upon binding to nucleic acids, thereby producing a bright red fluorescence in dead cells [20–22].

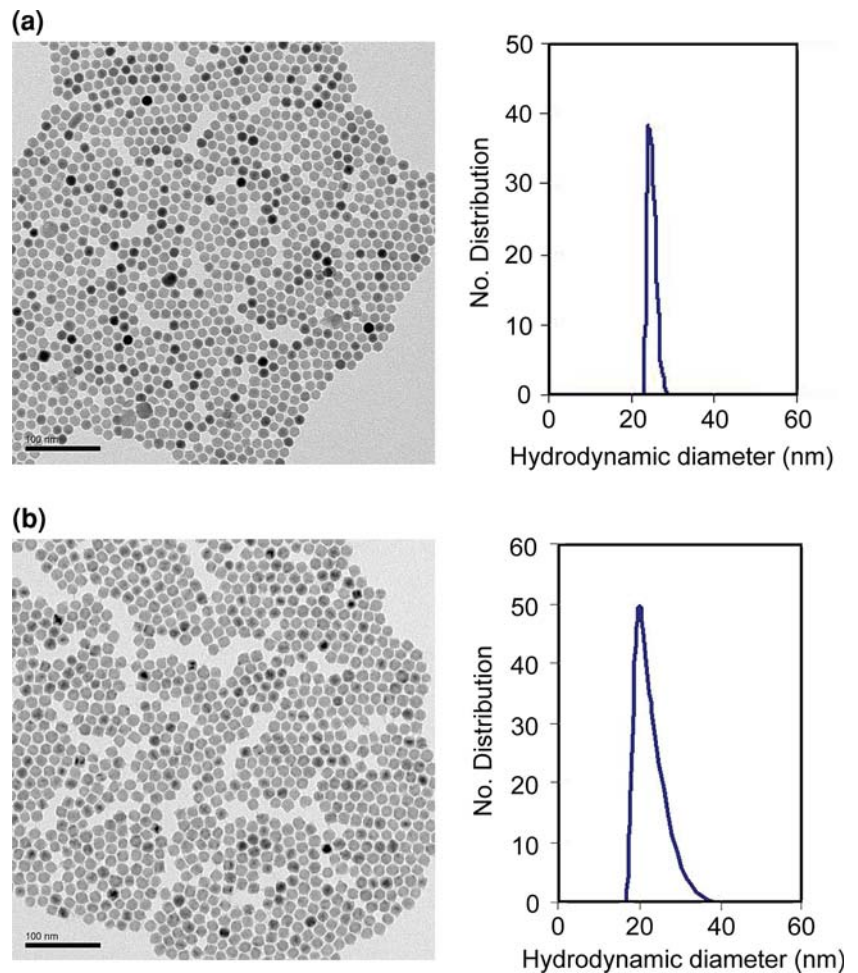
As a first step, A549 and MCF7 cells were incubated with different concentrations of  $\text{Fe}_3\text{O}_4$  and  $\text{MnO}$  nanoparticles for 18 h to determine the screening concentration range in our conditions. In some references, the uncoated  $\text{Fe}_3\text{O}_4$  had an effect on the viability of PC12 neuronal cells more than 0.15 mM concentration, inhibiting the normal

formation of cell morphology [23]. Other reports presented various concentrations of  $\text{Fe}_3\text{O}_4$  showing the cytotoxicity such as 0.05 and 0.25 mg/ml [24–26], depending on the sizes of nanoparticles and assay methods. Meanwhile,  $\text{Fe}_3\text{O}_4$  with biocompatible surface modification revealed cytotoxicity with much higher concentration. For example, 10 mg/ml concentration of  $\text{Fe}_3\text{O}_4$  coated with a Ferumoxtran-10 exhibited low cytotoxicity when treated with human monocyte–macrophages [27]. When the surface modification consisted of poly(maleic anhydride-*alt*-1-octadecene), it did not have any cytotoxicity less than 100 mM concentration [28]. Similarly as the coated  $\text{Fe}_3\text{O}_4$  nanoparticles,  $\text{IC}_{50}$  (half maximal inhibitory concentration: a measure of the effectiveness of a compound in inhibiting biological or biochemical function) value of  $\text{MnO}$  coated with PEG was 4.73 mM [9], while naked  $\text{MnO}$  had the cytotoxic effect more than 0.1 mg/ml [24], or 25  $\mu\text{M}$  [29]. Although the direct comparison of in vitro data of published reports is difficult due to the inconsistent cell lines, culturing conditions, and exposure times, it was helpful to decide a reasonable concentration range of PEG–phospholipid modified nanoparticle as 5–500  $\mu\text{g}/\text{ml}$  for concentration-dependent cytotoxic screening.

Figure 3 shows live (green)/dead (red) stain of (a)  $\text{Fe}_3\text{O}_4$ , (b)  $\text{MnO}$ , and (c) Feridex induced A549 and MCF7 cell lines for 18 h incubation with 5, 50, and 500  $\mu\text{g}/\text{ml}$  of concentration. To interpret the toxicity phenomena in a meaningful way, we used a medical contrast reagent, Feridex, as a control to evaluate the relative cytotoxic effect of  $\text{Fe}_3\text{O}_4$  and  $\text{MnO}$  nanoparticles on human cells. In all the cell images of Fig. 3, green fluorescence emission signal was dominant, showing that the cytotoxic effect of  $\text{Fe}_3\text{O}_4$  and  $\text{MnO}$  was not observed, the same as Feridex represented, and those engineered nanoparticles, thus, are stable enough to maintain the cells alive under the tested conditions. In the case of MCF7 cells treated with 5 and 50  $\mu\text{g}/\text{ml}$  concentration, some of them exhibited orange fluorescence, but this merged fluorescence detection may be derived from interference of green and red fluorescence signal caused by adhesion of EthD-1 to cell membrane because there was no signal of EthD-1 in the nucleus with  $\times 400$  enlarged images. These results demonstrated no significant cytotoxicity caused by  $\text{Fe}_3\text{O}_4$  and  $\text{MnO}$  treatment for 18 h incubation at 5–500  $\mu\text{g}/\text{ml}$  concentration. Please note that 500  $\mu\text{g}/\text{ml}$  is considered as extremely high concentration for cytotoxicity test, and the results prove the excellent stability and biocompatibility of PEG–phospholipid encapsulated  $\text{Fe}_3\text{O}_4$  and  $\text{MnO}$ . Encouraged by the previous data, we prolonged the incubation time to 2 and 4 days with the highest concentration of 500  $\mu\text{g}/\text{ml}$  to test cytotoxicity expression under harsh conditions.

Figure 4 shows the relative live percent of cells after 2 and 4 day incubation with 500  $\mu\text{g}/\text{ml}$  concentration of

**Fig. 2** Transmission electron microscopic (TEM) images and hydrodynamic diameter diagrams. **a** Fe<sub>3</sub>O<sub>4</sub> nanoparticles; **b** MnO nanoparticles. Scale bar = 100 nm



MnO, Fe<sub>3</sub>O<sub>4</sub>, and Feridex. The cytotoxicity of control experiments in which an incubation step with nanoparticles was omitted was calculated as 100% according to the below equation, and relative live percent of cells of other nanoparticles compared with that of control was recorded:

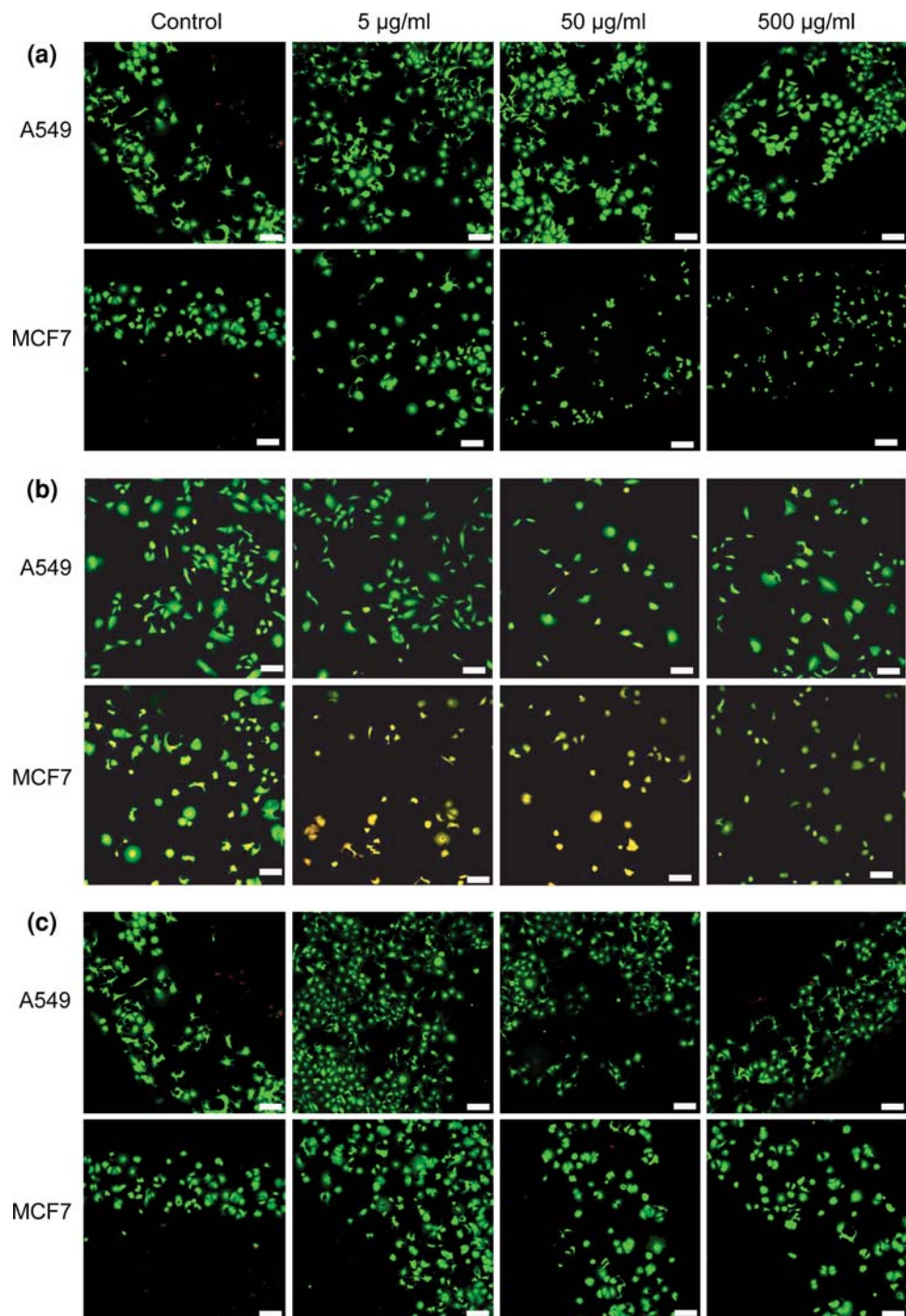
$$\% \text{ Live Cells} = \frac{F(530)_{\text{sam}} - F(530)_{\text{min}}}{F(530)_{\text{max}} - F(530)_{\text{min}}} \times 100\%$$

where  $F(530)_{\text{sam}}$  is the fluorescence intensity of the samples at 530 nm where cells are stained with calcein AM and EthD-1;  $F(530)_{\text{max}}$  the fluorescence intensity of the control at 530 nm where all cells are alive stained with calcein AM;  $F(530)_{\text{min}}$  the fluorescence intensity of the control at 530 nm where all cells are dead stained with EthD-1.

In Fig. 4a, cytotoxicity of MnO nanoparticles affected cell viability most significantly upon A549 and MCF7 cells, while Feridex showed the highest live percent of cells. In case of T98G cells, the cell viability treated with Fe<sub>3</sub>O<sub>4</sub> was higher than that of Feridex. However, after 4 days incubation (Fig. 4b), the absolute viability value is improved and the difference of relative live percent of cells of three nanoparticles becomes minimized. During the prolonged

incubation time from 2 to 4 day, the number of live cells was multiplied due to the cell division of which the period is approximately 24–48 h. In addition, the concentration of nanoparticles gradually decreases by the cellular uptake of nanoparticles into the cytoplasm through the endocytosis process. Thus, the newly born-cells by cell division are exposed to relatively low concentration of nanoparticles, and increase the  $F(530)_{\text{sam}}$  factor in a numerator, resulting in the cell viability was close to the control value after 4 day incubation. Similarly, when treated with poly(ethyleneglycol) monomethacrylate (PEGMA)-coated magnetic nanoparticles (MnFe<sub>2</sub>O<sub>4</sub> and Fe<sub>2</sub>O<sub>3</sub> core/polystyrene shell), the viability of macrophages also increased as the incubation time increased from 3 to 5 days [30]. Whereas the pattern of A549 cell viability after 4 day incubation was similar to that of 2 day, the viability of MnO- and Fe<sub>3</sub>O<sub>4</sub>-treated cells showed 45 and 19% increase compared with the control and that of Feridex-treated cells showed 12% decrease. In the set of MCF7 cells, the viability of MnO, Fe<sub>3</sub>O<sub>4</sub>, and Feridex-treated cells showed 18, 23, and 7% increase, respectively, and the lowest cytotoxicity was represented with Fe<sub>3</sub>O<sub>4</sub> rather than Feridex. In case of T98G, the cell viability of all

**Fig. 3** Laser scanning confocal microscopic images of the cells treated with the live/dead cell assay kit after 18 h of incubation with nanoparticles. **a**  $\text{Fe}_3\text{O}_4$ -treated A549 (*upper panel*) and MCF7 cells (*lower panel*); **b** MnO-treated A549 and MCF7 cells; **c** Feridex-treated A549 and MCF7 cells at indicated concentrations. Green fluorescent emission was dominated in all the cells, suggesting low cytotoxic effect on the cells. Scale bar = 20  $\mu\text{m}$



the nanoparticles after 4 day incubation was close to that of the control, and the percent of live cell treated with MnO increased significantly. As the incubation time is expanded from 2 to 4 days, the rate of viability increase is much larger with MnO and  $\text{Fe}_3\text{O}_4$  than Feridex. This result suggested that PEG-derivatized phospholipid confers nanoparticles high biocompatibility as well as higher stability than that of Feridex to minimize the metal ion leakage for 4 days. Another notable phenomenon is that the drastic viability

recovery of T98G cells after 4 day incubation under MnO treatment. This result may be attributed to the unique property of glioma T98G cell line. Manganese is mainly used as components for metalloproteins, mitochondrial enzymes, Mn-superoxide dimutase, pyruvate carboxylase, glutamine synthetase, and so on [31]. Especially, in case of glioma cells like T98G, the receptor for manganese is highly developed to enable the manganese components to penetrate the cell membrane through endocytosis with ease.

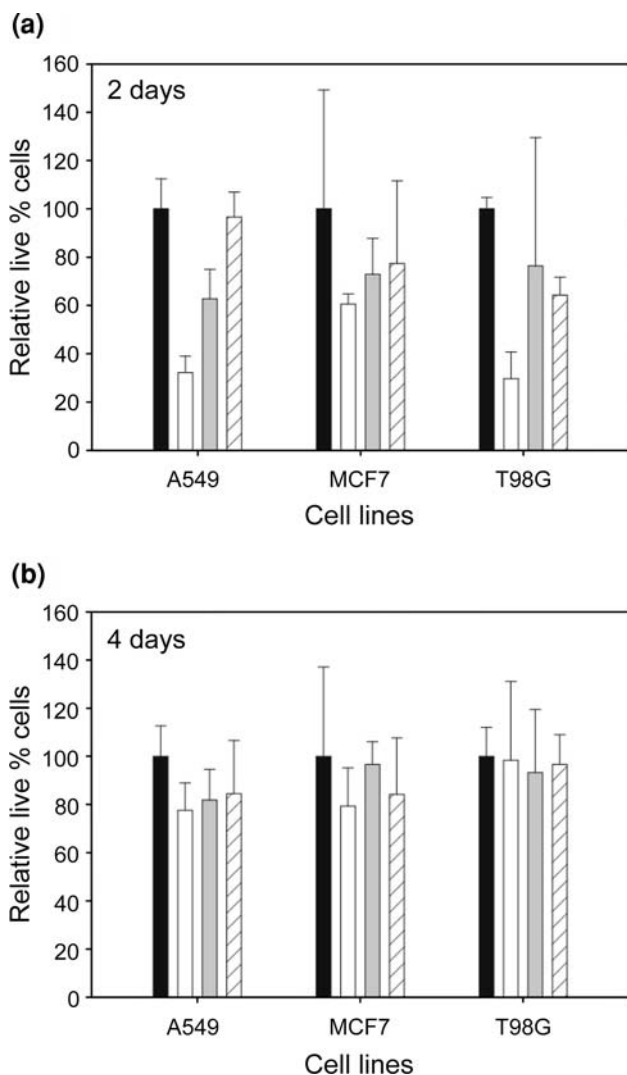


**Fig. 4** Cytotoxic effects of nanoparticles on human cells (A549, MCF7, and T98G) treated with the live/dead cell assay kit after 2 and 4 days of incubation with 500 µg/ml concentration of nanoparticles. (control: ■, MnO: □, Fe<sub>3</sub>O<sub>4</sub>: ■, Feridex: ▨)

Those properties could explain why cell viability treated with MnO nanoparticles on T98G is recovered drastically after 4 day incubation.

As a consequence, PEG–phospholipid encapsulated Fe<sub>3</sub>O<sub>4</sub> and MnO nanoparticles revealed cytotoxicity after 2 day incubation with 500 µg/ml concentration, and MnO represented more cytotoxic effect than Fe<sub>3</sub>O<sub>4</sub>. As incubation time increased to 4 days, the relative cell viability with Fe<sub>3</sub>O<sub>4</sub> and MnO has improved compared with that of a control mainly due to the cell doubling, and the recovery rate for Fe<sub>3</sub>O<sub>4</sub> and MnO is much larger than a medical contrast reagent, Feridex, which means high stability of nanoparticles for a long time. In general, the phospholipid–PEG encapsulated Fe<sub>3</sub>O<sub>4</sub> exhibited equivalent or better cell viability than Feridex, demonstrating a potential as an advanced MRI contrast agent.

Cytotoxicity survey using LDH assay

Cell membrane damage caused by nanotoxicity leads to the release of cytoplasmic enzymes, and the measurement of LDH release is a well-accepted assay to estimate cell membrane integrity and quantify cell cytotoxicity [32–36]. LDH leakage measurement uses resazurin as a fluogenic indicator for measuring the activity of LDH released from damaged cells [37]. Released LDH transfers lactate to pyruvate with co-reaction of NAD<sup>+</sup> to NADH transition, and then the oxidation reaction of NADH to NAD<sup>+</sup> transfers the non-fluorescent resazurin to red fluorescent resorufin [37]. Viable cells, however, produce negligible fluorescent signal with LDH assay.

Based upon the results of live/dead cell assay, cytotoxicity of nanoparticles was investigated with LDH assay at highest concentration of nanoparticles (500 µg/ml) and incubation time (2 and 4 days) (Fig. 5). In Fig. 5a, the relative cytotoxicity data of A549 cells were similar to those of live/dead cell assay, showing the order of cytotoxicity is MnO > Fe<sub>3</sub>O<sub>4</sub> > Feridex, which trend was also maintained at 4 day incubation. Almost same level of cytotoxicity of all the nanoparticles was expressed with MCF7 cells after 2 day incubation, but MnO became the most toxic after 4 day following the cytotoxic order of A549 as shown in Fig. 5b. However, in case of T98G, unexpectedly Fe<sub>3</sub>O<sub>4</sub> resulted in the highest toxic effect after both 2 and 4 days, and the overall cytotoxicity level is higher than other cell lines. As incubation time was expanded from 2 to 4 days, the relative percent of cytotoxicity based on the LDH assay increased 13% except for A549 cells, whereas the cell viability also increased in proportion to the incubation time as shown in Fig. 4. This discrepancy can be interpreted as the different principle between a live/dead viability test and a LDH leakage assay. A LDH leakage assay measures the fluorescent signal of membrane-damaged cells, not the live normal ones, while the live/dead assay considers the fluorescent signal of live cells, too. Therefore, even though the cell number is doubling as incubation time is more than 2 days, the LDH leakage assay cannot count the viability of live ones, but only detect the accumulated LDH derived from continuous leakage of damaged cells which number is proportional to the time. That explains why T98G cells treated with MnO shows slightly (10%) increased cytotoxicity with incubation time from 2 to 4 days (Fig. 5), while the cell multiplication and unique receptor of the glioma T98G cells significantly contributed to the improved cell viability evaluated by live/dead cell assay. From the LDH assay experiments, it is concluded that the MnO and Feridex nanoparticle are the highest and lowest cytotoxic to human cell lines, respectively, and the overall toxicity level increases as incubation time prolonged.

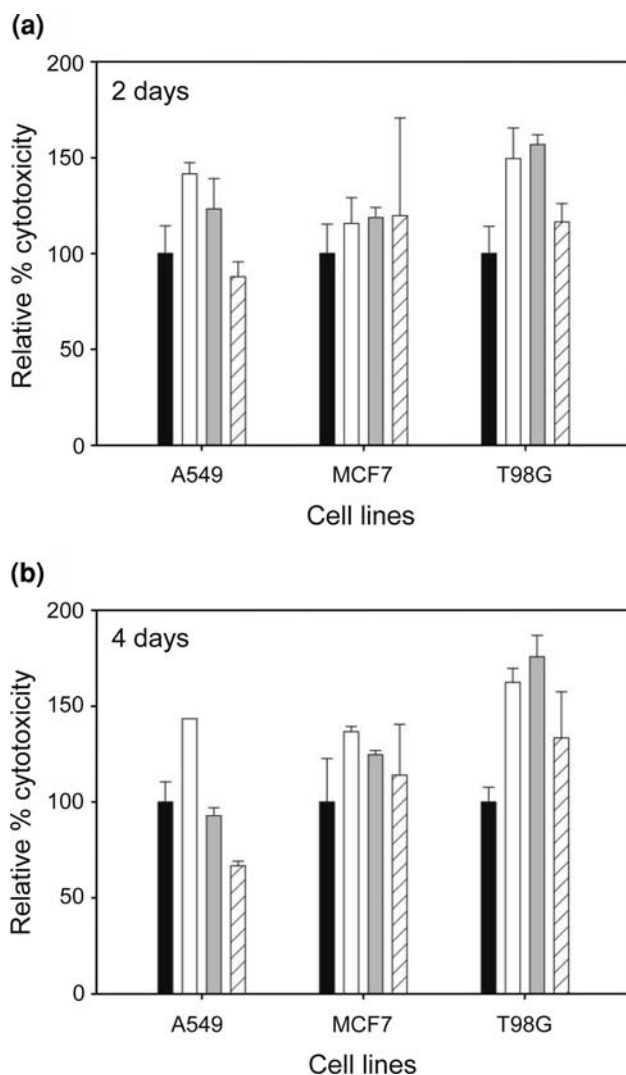


**Fig. 5** Cytotoxic effects of nanoparticles on human cells (A549, MCF7, and T98G) treated with the LDH assay kit after 2 and 4 days of incubation with 500 µg/ml concentration of nanoparticles. (control: ■, MnO: □, Fe<sub>3</sub>O<sub>4</sub>: ▒, Feridex: ▨)

#### Oxidative stress level survey using a ROS detection kit

The ROS detection assay is based on carboxy-H<sub>2</sub>DCFDA, a reliable fluorogenic marker for ROS in live cells [38, 39]. Under oxidative stress conditions, ROS production is dramatically increased, resulting in subsequent alteration of membrane lipids, protein, and nucleic acids. The nonfluorescent carboxy-H<sub>2</sub>DCFDA permeates live cells and is deacetylated by nonspecific intracellular esterases. In the presence of ROS particularly produced during oxidative stress, the reduced fluorescein compound is oxidized and emits bright green fluorescence [38, 39]. It is reasonable to perform oxidative stress evaluation since the metal oxide nanoparticles have a potential to generate ROS. We selected A549 cells and MnO as a representative for ROS

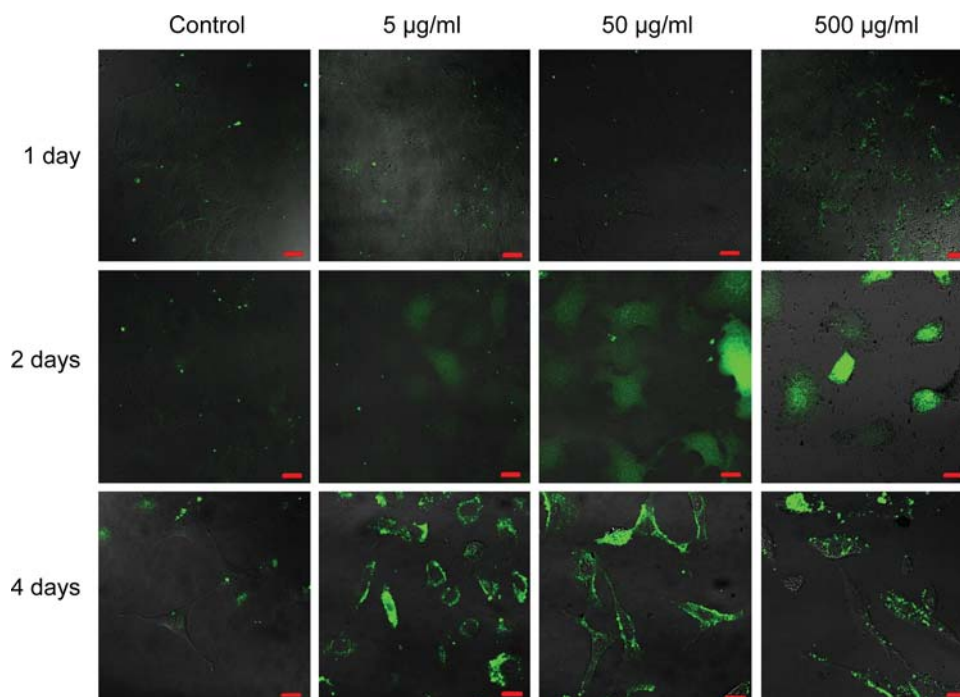
test, which showed reduced cytotoxicity in both live/dead cell assay and LDH assay as incubation time increased from 2 to 4 days. Confocal microscopic images of ROS generation were displayed in Fig. 6 depending on the 1, 2, and 4 day exposure to MnO with concentration of 0, 5, 50, and 500 µg/ml. One-day incubation produced a minimal ROS level, while 2-day incubation represented a significant ROS and then the expression level was diminished after 4 days, which trend is matched with that of live/dead cell viability and LDH test on A549 cells. These results can be explained by induction of an active glutathione (GSH) reductase and glucose-6-phosphate dehydrogenase [31]. These enzymes reduce the glutathione disulfide (GSSG) to GSH, an oxidized form of GSSG. The produced GSHs can lessen the concentration of reactive oxygen species by donating the protons and electrons with conversion of GSH to the oxidized form, GSSG. In other words, the ROS level started to decrease from 2 days by the continuous activity of such enzymes, supported by previous studies showing that GSH concentration of A549 cells treated with cerium oxides decreased up to 2 days, and then started to increase from 3 days [40]. Notably, the ROS level is proportional to the concentration of nanoparticles, and dose-dependent increase of oxidative stress was clearly demonstrated at 2 day incubation. At high concentration of MnO, the expression and activity of glutathione (GSH) reductase and glucose-6-phosphate dehydrogenase will be augmented to offset the generated ROS. This could interpret the similar green fluorescent emission intensities after 4 day incubation regardless of the MnO concentration, although detailed researches on the enzyme activity and kinetics are necessary to clarify the ROS expression mechanism.

#### Conclusion

In this study, we conducted cytotoxicity screening of PEG-derivatized phospholipid coated Fe<sub>3</sub>O<sub>4</sub> (12 nm) and MnO (14 nm) metal oxide nanoparticles by varying the concentration, incubation time, human cell lines, and viability/cytotoxicity assay. The surface chemistry with PEG-phospholipid modification provides the advanced monodispersity, biocompatibility, water-solubility, and stability in an aqueous media, so that the resultant cytotoxic effect was minimal in one day incubation even at high concentration (500 µg/ml). Under the harsh conditions with longer incubation time and high concentration, the MnO nanoparticle generally represented higher level of toxicity, whereas cytotoxicity of Fe<sub>3</sub>O<sub>4</sub> is equivalent or better than the commercial medical contrast reagent, Feridex, based on the live/dead cell viability assay. In addition, the PEG-modified MnO and Fe<sub>3</sub>O<sub>4</sub> exhibited better stability than Feridex for a prolonged incubation time. In the LDH



**Fig. 6** Laser scanning confocal microscopic images of the A549 cells treated with the ROS detection kit after 1, 2, and 4 days of incubation with 5, 50, and 500  $\mu\text{g/ml}$  concentrations of MnO. No significant fluorescent signal was detected after 1 day incubation, while green fluorescent emission for 2 days was intensified and then reduced after 4 day incubation. Scale bar = 20  $\mu\text{m}$



leakage assay, the absolute number of membrane-damaged cells is proportional to the incubation time, resulting in the increase of cytotoxicity of all the nanoparticles on the human cell lines. However, the lung, breast, and neuron cells exhibited somewhat different pattern of cytotoxic effect, indicating that studies on unique cell properties and cell biology related to the interaction with nanoparticles are necessary to elucidate the mechanism of cytotoxicity. The ROS expression level was involved with the activity of glutathione (GSH) reductase and glucose-6-phosphate dehydrogenase. While 2 day incubation of MnO on the lung cancer cells shows higher and dose-dependent increase of oxidative stress, 4 day incubation exhibited the reduced and dose-independent ROS expression. Although in vitro results need to be validated in in vivo system, these in vitro studies strongly suggest a bright prospect of PEG-phospholipid coated  $\text{Fe}_3\text{O}_4$  and MnO nanoparticles for practical application in nanomedicine because of their unique electronic properties and the relatively low toxicity.

**Acknowledgments** This research was supported in part by the Korea Science and Engineering Foundation (KOSEF) grant funded by the Korea government (MEST) (No. R11-2001-089-10002-0).

## References

- Lynch I, Dawson KA, Linse S (2006) Detecting cryptic epitopes created by nanoparticles. *Sci STKE* 327:pe14
- Colvin VL (2003) The potential environmental impact of engineered nanomaterials. *Nat Biotechnol* 21:1166–1170
- Warheit DB (2004) Nanoparticles: health impacts. *Mater Today* 7:32–35
- Adams LK, Lyon DY, Alvarez PJJ (2006) Comparative ecotoxicity of nanoscale  $\text{TiO}_2$ ,  $\text{SiO}_2$ , and ZnO water suspensions. *Water Res* 40:3527–3532
- Kagan VE, Bayir H, Shvedova AA (2005) Nanomedicine and nanotoxicology: two sides of the same coin. *Nanomedicine* 1:313–316
- Fischer HC, Chan WCW (2007) Nanotoxicity: the growing need for in vivo study. *Curr Opin Biotechnol* 18:565–571
- Linkov I, Satterstrom FK, Corey LM (2008) Nanotoxicology and nanomedicine: making hard decisions. *Nanomedicine* 4: 167–171
- Lewinski N, Colvin V, Drezek R (2008) Cytotoxicity of nanoparticles. *Small* 4:26–49
- Na HB, Lee JH, An K, Park YI, Park M, Lee IS, Nam D-H, Kim ST, Kim S-H, Sim S-W, Lim K-H, Kim K-S, Kim S-O, Hyeon T (2007) Development of a T1 contrast agent for magnetic resonance imaging using MnO nanoparticles. *Angew Chem Int Ed* 46:5397–5401
- Yin M, Brien SO (2003) Synthesis of monodisperse nanocrystals of manganese oxides. *J Am Chem Soc* 125:10180–10181
- Sun S, Zeng H (2002) Size controlled synthesis of magnetite nanoparticles. *J Am Chem Soc* 124:8204–8205
- Park J, An K, Hwang Y, Park J-G, Noh H-J, Kim J-Y, Park J-H, Hwang N-M, Hyeon T (2004) Ultra-large-scale syntheses of monodisperse nanocrystals. *Nat Mater* 3:891–895
- Medintz IL, Uyeda HT, Goldman ER, Mattoussi H (2005) Quantum dot bioconjugates for imaging, labelling and sensing. *Nat Mat* 4:435–446
- Bruchez M Jr, Moronne M, Gin P, Weiss S, Alivisatos AP (1998) Semiconductor nanocrystals as fluorescent biological labels. *Science* 281:2013–2016
- Wu H, Zhu H, Zhuang J, Yang S, Liu C, Cao YC (2008) Water soluble nanocrystals through dual interaction ligands. *Angew Chem Int Ed* 47:3730–3734
- White MA, Johnson JA, Koberstein JT, Turro NJ (2006) Towards the syntheses of universal ligands for metal oxide surfaces: controlling surface functionality through click chemistry. *J Am Chem Soc* 128:11356S–11357S

17. Selvan ST, Patra PK, Ang CY, Ying JY (2007) Synthesis of silica coated semiconductor and magnetic quantum dots and their use in the imaging of live cells. *Angew Chem Int Ed* 46:2448–2452
18. Kim BS, Qiu JM, Wang JP, Taton TA (2005) Magnetomicelles: composite nanostructures from magnetic nanoparticles and cross-linked amphiphilic block copolymers. *Nano Lett* 5:1987–1991
19. Dubertret B, Skourides P, Norris DJ, Noireaux V, Brivanlou AH, Libchaber A (2002) In vivo imaging of quantum dots encapsulated in phospholipid micelles. *Science* 298:1759–1762
20. Hayes AW (1994) Principles and methods of toxicology, 3rd edn. Raven Press, New York, pp 1231–1258
21. Papadopoulos NG, Dedoussis GVZ, Spanakos G, Gritzapis AD, Constantin N, Papamichail M (1994) An improved fluorescence assay for the determination of lymphocyte-mediated cytotoxicity using flow cytometry. *J Immunol Methods* 177:101–111
22. Kaneshiro ES (1993) Reliability of calcein acetoxymethyl ester and ethidium homodimer or propidium iodide for viability assessment of microbes. *J Microbiol Methods* 17:1–16
23. Pisanic TR, Blackwell JD, Shubayev VI, Finones RR, Jin S (2007) Nanotoxicity of iron oxide nanoparticle internalization in growing neurons. *Biomaterials* 28:2572–2581
24. Hussain SM, Hess KL, Gearhart JM, Geiss KT, Schlager JJ (2005) In vitro toxicity of nanoparticle in BRL 3A rat liver cells. *Toxicology In Vitro* 19:975–983
25. Gupta AK, Gupta M (2005) Cytotoxicity suppression and cellular uptake enhancement of surface modified magnetic nanoparticles. *Biomaterials* 26:1565–1573
26. Gupta AK, Wells S (2004) Surface-modified superparamagnetic nanoparticles for drug delivery: preparation, characterization, and cytotoxicity studies. *IEEE Trans Nanobiosci* 3:66–73
27. Muller K, Skepper JN, Posfai M, Trivedi R, Howarth S, Corot C, Lancelot E, Thompson PW, Brown AP, Gillard JH (2007) Effect of ultrasmall superparamagnetic iron oxide nanoparticles (Ferumoxtran-10) on human monocyte-macrophages in vitro. *Biomaterials* 28:1629–1642
28. Yu WW, Chang E, Sayes CM, Drezek R, Colvin VL (2006) Aqueous dispersion of monodisperse magnetic iron oxide nanocrystals through phase transfer. *Nanotechnology* 17:4483–4487
29. Chen JY, Tsao GC, Zhao Q, Zheng W (2001) Differential cytotoxicity of Mn(II) and Mn(III): special reference to mitochondrial [Fe-S] containing enzymes. *Toxicol Appl Pharmacol* 175:160–168
30. Hu F, Neoh KG, Cen L, Kang ET (2006) Cellular response to magnetic nanoparticles “PEGylated” via surface-initiated atom transfer radical polymerization. *Biomacromolecules* 7:809–816
31. Nordberg J, Arner ESJ (2001) Reactive oxygen species, antioxidants, and the mammalian thioredoxin system. *Free Radic Biol Med* 31:1287–1312
32. Mosmann T (1983) Rapid colorimetric assay for cellular growth and survival: application to proliferation and cytotoxicity assays. *J Immunol Methods* 65:55–63
33. Korzeniewski C, Callewaert DM (1983) An enzyme-release assay for natural cytotoxicity. *J Immunol Methods* 64:313–320
34. Arechabala B, Coiffard C, Rivalland P, Coiffard LJM, Roeck-Holtzauer YD (1999) Comparison of cytotoxicity of various surfactants tested on normal human fibroblast cultures using the neutral red test, MTT assay and LDH release. *J Appl Toxicol* 19:163–165
35. Roehn NW, Rodgers GH, Hatfield SM, Glasebrook AL (1991) An improved colorimetric assay for cell proliferation and viability utilizing the tetrazolium salt XTT. *J Immunol Methods* 142:257–265
36. Legrand C, Bour JM, Jacob C, Capiaumont J, Martial A, Marc A, Wudtke M, Kretzmer G, Demangel C, Duval D, Hache J (1992) Lactate dehydrogenase (LDH) activity of the number of dead cells in the medium of cultured eukaryotic cells as marker. *J Biotechnol* 25:231–243
37. Marzin D (1999) New approaches to estimating the mutagenic potential of chemicals. *Cell Biol Toxicol* 15:359–365
38. Maurer BJ, Metelitsa LS, Seeger RC, Cabot MC, Reynolds CP (1999) Increase of ceramide and induction of mixed apoptosis/necrosis by N-(4-hydroxyphenyl)retinamide in neuroblastoma cell lines. *J Natl Cancer Inst* 91:1138–1146
39. Konorev EA, Zhang H, Joseph J, Kennedy MC, Kalyanaraman B (2000) Bicarbonate exacerbates oxidative injury induced by antitumor antibiotic doxorubicin in cardiomyocytes. *Am J Physiol* 279:H2424–H2430
40. Lin W, Huang YW, Zhou XD, Ma Y (2006) Toxicity of cerium oxide nanoparticles in human lung cancer cells. *Int J Toxicol* 25:451–457